© 2019. Published by The Company of Biologists Ltd | Journal of Experimental Biology (2019) 222, jeb195578. doi:10.1242/jeb.195578

RESEARCH ARTICLE

Work loop dynamics of the pigeon (*Columba livia*) humerotriceps demonstrate potentially diverse roles for active wing morphing

Jolan S. Theriault[1], Joseph W. Bahlman[2], Robert E. Shadwick[1] and Douglas L. Altshuler[1,*]

ABSTRACT

Control of wing shape is believed to be a key feature that allows most birds to produce aerodynamically efficient flight behaviors and high maneuverability. Anatomical organization of intrinsic wing muscles suggests specific roles for the different motor elements in wing shape modulation, but testing these hypothesized functions requires challenging measurements of muscle activation and strain patterns, and force dynamics. The wing muscles that have been best characterized during flight are the elbow muscles of the pigeon (*Columba livia*). *In vivo* studies during different flight modes revealed variation in strain profile, activation timing and duration, and contractile cycle frequency of the humerotriceps, suggesting that this muscle may alter wing shape in diverse ways. To examine the multifunction potential of the humerotriceps, we developed an *in situ* work loop approach to measure how activation duration and contractile cycle frequency affected muscle work and power across the full range of activation onset times. The humerotriceps produced predominantly net negative power, likely due to relatively long stimulus durations, indicating that it absorbs work, but the work loop shapes also suggest varying degrees of elastic energy storage and release. The humerotriceps consistently exhibited positive and negative instantaneous power within a single contractile cycle, across all treatments. When combined with previous *in vivo* studies, our results indicate that both within and across contractile cycles, the humerotriceps can dynamically shift among roles of actuator, brake, and stiff or compliant spring, based on activation properties that vary with flight mode.

KEY WORDS: Flight, Active wing morphing, Wing muscle, Muscle function, Work loop, Pigeon

INTRODUCTION

The avian wing undergoes substantial shape change during both flapping and gliding (Altshuler et al., 2015; Lentink et al., 2007; Pennycuick, 1968, 2015). The ability to alter wing shape allows birds to control their aerodynamic efficiency (Lentink et al., 2007), and is also hypothesized to contribute to their maneuverability in flight (Altshuler et al., 2015). Some of the change in wing shape is caused by passive tension in soft tissue and inertial forces during flapping, but some shape change is expected to be under active control of the muscles intrinsic to the wing (Chin et al., 2017; Dial, 1992a; Vazquez, 1994). However, most research of avian flight muscles has focused on the two large, bilateral muscles in the pectoral region, which only have their insertions in the wing.

The pectoral muscles, the pectoralis major and the supracoracoideus, power the down- and up-strokes, respectively and have been characterized through *in vivo* measurements of activation, strain and force. These measurements have demonstrated their primary roles as actuators (Biewener et al., 1998a; Dial, 1992a,b; Ellerby and Askew, 2007a; Robertson and Biewener, 2012; Tobalske, 2007) with contributions to braking and elastic storage during wing turnaround (Biewener et al., 1998a; Dial, 1992b). The specific roles of the muscles intrinsic to the wing are largely unknown. Although anatomical measurements provide general hypotheses for wing muscle functions (Chin et al., 2017; Dial, 1992b; Robertson and Biewener, 2012), measurements of length and force dynamics are required to determine their contributions to wing morphing.

It is challenging to record activation and strain from intrinsic muscles, due to smaller size, increased distance from the body, and, in the case of flapping, high wingbeat frequency. The most extensive muscle activation measurements were performed by Dial and colleagues (Dial et al., 1991). Electromyogram recordings (EMGs) from 11 muscles in the European starling (*Sturnus vulgaris*), including 9 intrinsic wing muscles, were made during forward flight in a wind tunnel (Dial et al., 1991). EMGs from 17 muscles in the pigeon (*Columba livia*), including 15 intrinsic to the wing, were made during takeoff, ascending, forward flight, descending and landing (Dial, 1992b). These studies revealed that all of the wing muscles were active during flapping flight, but with considerable variation within and among muscles.

Only one study has included measurements of fascicle strain from intrinsic wing muscles: Robertson and Biewener (2012) obtained EMG recordings and sonomicrometry fascicle strain measurements from pigeons, in the pectoralis major and in the antagonist muscles that span the avian elbow. From this effort, activation and fascicle strain data are available from the humerotriceps, scapulotriceps and biceps brachii, as the birds went through a sequence of takeoff, forward flight and landing. These *in vivo* measurements are consistent with the hypothesis that the muscles control flexion, extension and stabilization of the avian elbow (Dial, 1992b; Robertson and Biewener, 2012). Control of the elbow joint angle should be important for adjusting wing shape during gliding, stabilizing the wing during the downstroke, and folding the wing during the upstroke to minimize counter-productive forces. However, demonstration of this hypothesis requires measurements of muscle force, work and power (e.g. Ellerby and Askew, 2007a; Roberts and Azizi, 2010).

Here, we build upon the *in vivo* measurements of muscle activation and fascicle strain obtained by Robertson and Biewener (2012) to measure muscle force in the pigeon humerotriceps. We focused on the humerotriceps because its anatomy and accessibility make it well suited for the work loop procedure. The humerotriceps

[1]Department of Zoology, University of British Columbia, 4200-6270 University Blvd, Vancouver, BC V6T 1Z4, Canada. [2]Department of Biology, California State University, Sacramento, 6000 J St., Sacramento, CA 95819, USA.

*Author for correspondence (doug@zoology.ubc.ca)

J.S.T., 0000-0002-8673-8406; J.W.B., 0000-0002-7870-5479; R.E.S., 0000-0002-5039-8606; D.L.A., 0000-0002-1364-3617

Received 31 October 2018; Accepted 14 March 2019

is a bipennate muscle that originates on the head of the humerus, and in the pneumatic fossa that is located on the ventral side of the head of the humerus, and inserts onto the olecranon process at the proximal end of the ulna on the dorsal side (Chatterjee, 2015; Robertson and Biewener, 2012). Short tendons should produce very little stretch independently of the muscle itself, thereby causing a negligible delay between force production and motion (Konow et al., 2015; Sawicki et al., 2015). At the insertion, the humerotriceps has a short length of tendon (~0.5 mm) that extends beyond muscle fibre attachment. We therefore assumed that this portion of tendon that extends beyond muscle fibre attachment was too short and stiff to contribute a substantial amount of stretch. However, we appreciate that this may not necessarily be true for this particular muscle–tendon unit. We took advantage of these anatomical features to modify an *in situ* work loop approach (Nelson et al., 2004; Roberts and Azizi, 2010) because it is not currently feasible to develop an *in vivo* force measurement technique specific to any of the elbow muscles for which activation and strain data are available.

In situ work loop experiments allow for measurement of muscle performance space, both within and beyond the range of observed parameters from *in vivo* studies (Josephson, 1985). However, it is not feasible to explore every aspect of potential variation because of degradation in muscle force following multiple trials. We focused on two manipulations that were tested across the full range of activation phases because the functions of cyclic muscles are highly dependent on onset of motor activation relative to the length-change cycle (Ahn and Full, 2002; Dickinson et al., 2000; Josephson, 1985; Roberts et al., 1997; Sawicki et al., 2015). The two focal manipulations were chosen based on the potential shift in muscle role over the range of observations from *in vivo* studies: (1) we tested two stimulus durations that were representative of the 52–74% of the wingbeat cycle range of activation periods that was observed during previous electromyogram recordings from the pigeon humerotriceps (Dial, 1992b; Robertson and Biewener, 2012); (2) we tested three cycle frequencies that were representative of the 5–10 s^{-1} range that was observed during previous measurements of wingbeat kinematics (Berg and Biewener, 2008, 2010; Dial, 1992b; Robertson and Biewener, 2012; Usherwood et al., 2011) (Table 1). These results were compared with the *in vivo* range of values to gain insight into what possible functions the pigeon humerotriceps can perform during different modes of flapping flight.

Duration of humerotriceps muscle activation is an important aspect to probe because it has been shown to occupy over half of its contractile cycle, making it likely that this muscle produces force during both lengthening and shortening. Therefore, each cycle could conceivably contain elements of both positive and negative work. However, it is uncertain how this might affect the *in vivo* function of this muscle. The wingbeat cycle frequency is also an important aspect to probe because it effectively dictates the contractile cycle frequency of all of the wing muscles, including the humerotriceps (Robertson and Biewener, 2012). A muscle's contractile cycle frequency determines its lengthening and shortening velocities, which would affect the muscle's ability to produce work and power, depending on its inherent properties such as its force–velocity relationship.

MATERIALS AND METHODS

Animals

Work loop experiments were performed with four female and five male pigeons [*Columba livia* (Gmelin 1789)] acquired from a local breeder (Aldergrove, BC). Body mass was 329.5±6.0 g (mean±s.e.m.) for females, and 318±25.7 g for males. Birds were housed at the University of British Columbia in wire cages with a 12 h light:12 h dark cycle and *ad libitum* access to premium pigeon seed mix, water, mineral and iodine grit, and calcium-enriched grit. All birds that served as experimental subjects for this study were

Table 1. Flight and muscle variables

		Wingbeat		Activation		
Study	Flight mode	Frequency (s^{-1})	Duration (ms)	Avg. duration (% wingbeat)	Duration (ms)	Onset (% cycle relative to peak fascicle length)
Robertson and Biewener, 2012‡	Takeoff	8.6§	116§	67	78	5–10¶; −6 to −1‡‡
	Level flight			65	76	8–12¶; −8 to −4‡‡
	Landing			68	79	8–12¶; −4 to 0‡‡
Usherwood et al., 2011*	N/A	5–10	200–100	N/A	N/A	N/A
Berg and Biewener, 2010‡	Takeoff	7.1–9.2	113–130	N/A	N/A	N/A
	Level flight	6.57±0.30	152±3.33			
	Landing	6.1–8.0	128–147			
Berg and Biewener, 2008‡	Ascent and descent	6.1–9.6	104–164	N/A	N/A	N/A
Biewener et al., 1998a‡	Level flight	8.70±0.26	115±3.85	N/A	N/A	N/A
Dial, 1992b‡,§§	Takeoff	9.1 (8.3–10)	110	56	61	38–49**; 28–38‡‡
	Ascent	9.4 (9–10.1)	106	52	55	42 to −47**
	Level flight	8.5 (7.6–9.3)	118	57	67	12–17**; −4 to 1‡‡
	Descent	8.4 (7.7–9.5)	119	74	88	6–7**
	Landing	8.3 (7.5–9.3)	120	52	62	36–49**; 24–37‡‡

*Free-flying pigeons; ‡Captive, trained pigeons; §Values averaged across flight modes. ¶Ranges calculated using average humerotriceps peak fascicle length (% relative to the wingbeat cycle) and the onset timings reported by Robertson and Biewener (2012).

**Ranges calculated using average humerotriceps peak fascicle length (% relative to the wingbeat cycle) reported by Robertson and Biewener (2012) and onset timings reported by Dial (1992b), who defined the wingbeat cycle using kinematics of wingtip excursion and set the start of each wingbeat cycle as the onset of pectoralis activation. To justify using strain data from Robertson and Biewener (2012), wingbeat cycle was adjusted to reflect pectoralis shortening using Hedrick et al. (2003)'s quantification of the difference between the two wingbeat cycle definitions, so that Dial (1992b)'s wingbeat cycle and onset timings were on the same scale and timing as the Robertson and Biewener (2012) study.

‡‡Ranges determined using the humerotriceps peak fascicle length (% relative to the wingbeat cycle) calculated from raw sonomicrometry data (Robertson and Biewener, 2012), across each flight mode.

§§All values estimated from published figures, and used to calculate activation duration as percentage wingbeat cycle, and average wingbeat frequency and duration (figs 8 and 10, respectively in Dial, 1992b).

Journal of Experimental Biology (2019) 222, jeb195578. doi:10.1242/jeb.195578

euthanized at the end of the procedure. All procedures were approved by the University of British Columbia Animal Care Committee.

Surgical procedure

We developed an *in situ* work loop technique to study whole muscle performance in the pigeon wing while maintaining normal body temperature and the flow of nutrients and oxygen through an intact blood supply (Nelson et al., 2004). Anesthesia was induced by 4% isoflurane administered via a gas vaporizing system with a 50:50 mix of pure oxygen and nitrogen delivered at a combined flow rate of 1 l min^{-1}. Maintenance anesthesia level was held with 0.6–1.7% isoflurane throughout the procedure, which lasted up to 6–10 h for useful data collection. An analgesic, 10% (v/v) butorphanol (1 µl g^{-1} of body mass), was administered intramuscularly via the pectoralis within an hour of induced anesthesia. A half-dose of the analgesic was given 4–5 h after the initial dose. Additionally, 3 ml of 0.9% (w/v) unbuffered saline was administered subcutaneously near the nape of the neck every 2–3 h during surgery and just prior to the start of data collection. Any exposed tissue was covered with 0.9% (w/v) saline-soaked cotton and irrigated regularly throughout the procedure with warm saline.

To prevent interference from contractions of other wing muscles, we isolated most of the humerotriceps muscle in the right wing from surrounding muscles without causing damage to the blood vessels and nerves that supply it. The origin of the humerotriceps, located on (and in) the head of the humerus, and the insertion of its short tendon on the proximal end of the ulna were left intact. Two 1.8 mm holes were drilled in the humerus, one at the distal end and one 1.5 cm proximally, and zero gauge bolts were passed through these holes and screwed into pre-tapped holes in a 6.4 mm (1/4 inch) thick aluminum block mounted on acrylic (Fig. 1A). The entire setup was then fastened to a breadboard with a 2.5 cm (1 inch) hole pattern. We used this method to immobilize the humerus and consequently the origin of the humerotriceps because we had determined that it was sufficient for eliminating undesired movement of these elements during the initial stages of experimental development. A short section of the ulna that contained the tendon insertion of the humerotriceps was isolated and tied to a non-compliant, 0.20 mm, thermally bonded thread (Wildfire 162U-008, Beadalon, Valley Twp, PA). The other end of the thread was tied through a hole on a lever arm connected to a dual-mode lever system arm (Fig. 1A). Both knots were sealed with cyanoacrylate to prevent slippage. The muscle temperature was maintained at 36–41°C throughout the experiments with an external heat source. After the end of each experiment, the humerotriceps muscle was extracted to measure its length and mass.

The muscle was activated by stimulating the dorsal branch of the brachial nerve supplying the humerotriceps (King and McLelland, 1984). The nerve was exposed and isolated by incising and reflecting the right pectoralis major, tied with 6-0 silk suture, and severed just distal to the point of emergence from the thoracic cavity (Nelson et al., 2004). The nerve was then draped over a bi-polar nerve hook, made from two insulated (HML) silver wires (California Fine Wires, Grover Beach, CA) with 1 cm exposed tips that were curved (Fig. 1A). The two wires were housed in a small syringe with the exposed tips protruding from the tapered end. The nerve was coated in mineral oil to prevent desiccation without generating a salt bridge between the two electrodes.

We monitored the activation and condition of the humerotriceps muscle using electromyography (EMG) to record the induced muscle potentials throughout the experiments (Fig. S1). We made

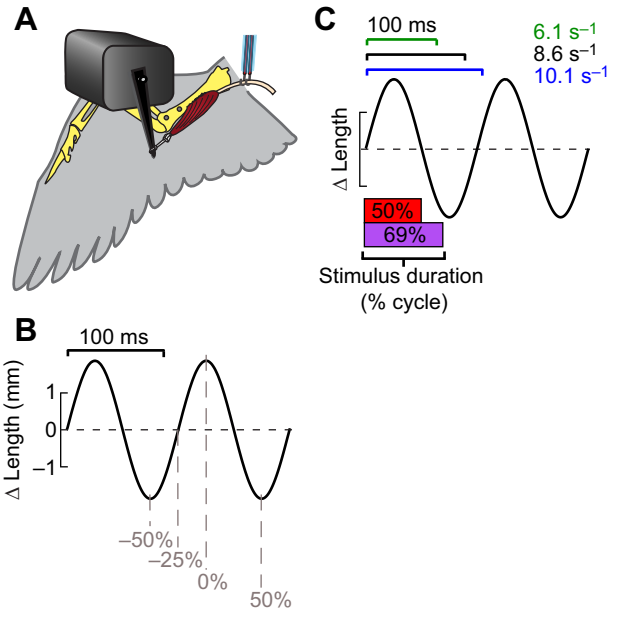

Fig. 1. *In situ* work loop preparation for testing the contractile properties of pigeon humerotriceps muscles. (A) The humerotriceps muscle originates on the head of the humerus and, during the *in situ* work loop experiments, the insertion is attached to the servo motor arm. Circles indicate where screws were drilled into the humerus to immobilize it. The dorsal branch of the brachial nerve was draped over two hooked electrodes and received an electrical impulse to stimulate the humerotriceps. (B) A sample 8.6 s^{-1} length-change cycle trace plotted over time, with gray dashed lines indicating where stimulus onset began for −50, −25, 0 (peak muscle length) and 50% phase. (C) Length-change trace with each of the three different frequency treatments denoted using the time scale bars in the top left: 6.1 s^{-1} (top, green); 8.6 s^{-1} (middle, black) and 10.1 s^{-1} (bottom, blue). The stimulus duty cycles are indicated by bars below the trace. Two different experiments were performed: (1) Contractile frequency was tested with 50% stimulus duty cycle (red stimulus bar). (2) Stimulus duty cycle [50% (red) versus 69% (purple)] was tested at a cycle frequency of 8.6 s^{-1}.

bipolar EMG electrodes from 3 µm diameter HML-insulated silver bifilar wire (California Fine Wires) with 1 mm tip exposure and 0.5 mm intertip distance (Dial, 1992b). These were inserted directly into the humerotriceps. A ground electrode was made from 4 µm diameter insulated silver BI wire (California Fine Wires) with 1 mm tip exposure, and inserted into the skin, between the left leg and the body.

In situ muscle data collection setup

To record force production and length changes in the humerotriceps muscle we used a Dual-Mode Lever System (Model 305C-LR, Aurora Scientific Inc., Aurora Ontario). This functions as both a force transducer and servo motor; in addition to recording force and position, it receives programmed input to impose the muscle length changes. The nerve-stimulating electrodes were connected to a High-Power Bi-Phase Current Stimulator (Model 701B, Aurora Scientific Inc., Aurora Ontario). The stimulus pattern was added to the experimental protocols written in Dynamic Muscle Control software (ASI 610A v5.415, Aurora Scientific Inc., Aurora Ontario). We programmed, ran and monitored all our work loop and parameter optimizing protocols, and treatment sequences using Dynamic Muscle Control. Data acquisition was done through an A/D signal interface (Model 604A, Aurora Scientific Inc., Aurora Ontario).

We recorded EMG output using a differential AC amplifier (Model 1700, A-M Systems, Sequim, WA). Live EMG data

monitoring was performed during trials using AxoScope (v10.5, Molecular Devices, Inc., Sunnyvale, CA) and a low-noise data acquisition system (Axon Instruments Digidata 1440A, Molecular Devices, Inc., Sunnyvale, CA). The EMG signals were also recorded by the same system that was used to acquire position and force (Aurora Scientific), allowing us to link the muscle activation pattern to the corresponding events in the position and force output traces.

Work loop parameters

We performed a set of parametric tests to optimize the performance of the humerotriceps muscle prior to work loop tests. We determined the stimulus intensity that generated maximum force through a series of two-pulse isometric contractions. Voltage was held at 60 V while current was increased (Lacourpaille et al., 2013) by increments of 1 mA until maximal force was achieved. We then increased the current by another 50%, and used this intensity for the remainder of the experiment (Josephson, 1997). This procedure should ensure full motor unit recruitment, while maintaining longevity of the muscle and nerve. We ran two tetanic contractions and one to two work loops to get an estimate of the maximum force production of the muscle, and to check that the muscle, the knot, the humerus were all secure and properly immobilized before starting the next phase of measurements to evaluate the force-length relationship of the muscle.

We evaluated the force–length relationship of the humerotriceps muscle to determine resting muscle length (L_0), using a series of two-pulse isometric contractions. We used doublet stimulation because each pulse within the doublet had a 0.2 ms duration and a frequency of 300 s^{-1}. Given that a stimulus train of 18 pulses did not produce tetany and that a stimulus train of 24 pulses was just enough to produce tetany, it seemed likely that a two-pulse stimulus for isometric contractions would produce negligible differences in force relative to a single pulse stimulus. Between measurements, we increased muscle length by 0.5–1 mm steps. We calculated the difference between the passive tension (baseline) and peak force (Josephson, 1997); this is also known as the developed force. The motor arm position and muscle resting length were then chosen based on a balance between maximized force production and low passive tension. This balance was determined when the developed force no longer exhibited an increase with increasing length. If there was no apparent developed force plateau, the muscle was lengthened until the increase in developed force was negligible relative to the previous length (i.e.: ∼50 mN) due to a near parallel rise in passive tension. In these cases, the shorter of the two muscle lengths exhibiting similar developed forces was chosen as L_0. We also used the two-pulse isometric contractions to evaluate the twitch kinetics of the humerotriceps. We measured the time for force to rise from 10% to 90% of its peak value and, subsequently, the time for force to relax from 90% to 10% of peak.

We used one standardized work loop protocol as the control to monitor the condition of the muscle and repeated this control work loop following each treatment. The settings for the control work loop protocol were 8.6 s^{-1} cycle frequency, stimulus duty cycle of 69% of the cycle, 8.7% strain amplitude and stimulus onset at −30% phase. The control work loop settings were chosen based on *in vivo* wingbeat frequency, stimulus duty cycle and fascicle strain amplitude (Robertson and Biewener, 2012). We chose the stimulus onset phase based on preliminary data that showed net positive work and power output consistently reached the highest values at −30% phase. Strain amplitude is the total percentage muscle length change relative to L_0 (Robertson and Biewener, 2012). We define stimulus onset relative to the length-change cycle, with 0% representing peak muscle length, and 50%/−50% representing minimum muscle length (Fig. 1B).

We chose to examine two work loop parameters in the humerotriceps that exhibited variation during *in vivo* recordings of pigeon flight (Dial, 1992b; Robertson and Biewener, 2012). These included stimulus duty cycle and wingbeat frequency (equivalent to the wing muscle length-change cycle frequencies). We chose our work loop treatment parameters using ranges that would reflect these observed variations, leading to four different treatments (Table S1).

We examined the effects of stimulus duration and wingbeat frequency by testing across the full range of stimulus phases, where stimulus timing was varied from −50 to 50% of the muscle length-change cycle at 5% intervals, for a total of 20 different stimulus onset phases. −50 and 50% are effectively the same stimulus onset but differ with respect to the number of proceeding cycles within a trial (Table S1). One adjustment was that 10% phase was replaced by 9% to represent the average *in vivo* activation onset reported by Robertson and Biewener (2012). All experiments presented in this study included measurements at each of the 20 different stimulus phases. Within each set of measurements, stimulus onset phases were tested in randomized order, and the same random order was held constant for each experimental treatment. Every experimental treatment started and ended with one cycle at −30% phase as an additional check for force degradation, for a total of 22 work loop trials per individual, per treatment.

We examined how stimulus duty cycle affected muscle performance by using two durations, 50% and 69% (Table S1). A 50% duty cycle represented *in vivo* EMG results from Dial (1992b), whereas 69% represented *in vivo* results from Robertson and Biewener (2012).

We next examined work loop cycle frequency while holding stimulus duty cycle constant at 50% (Table S1). Our standard length-change cycle frequency was based on the average frequency (8.6 s^{-1}) reported by Robertson and Biewener (2012). We examined two other frequencies, 6.1 and 10.1 s^{-1}, which represent the minimum and maximum wingbeat frequencies recorded from multiple flight modes in pigeons, across several studies.

Strain amplitude, nerve stimulus pulse duration, pulse frequency and the number of strain cycles per trial were held constant across all treatments. Strain amplitude was approximated because muscle L_0 could not be accurately measured until after the experiments were completed, due to the portion of the humerotriceps' origin that is located inside the head of the humerus, which made full excision necessary for determining muscle length. Therefore, we determined the strain amplitude to be used for all work loops by calculating 8.7% of the average resting length of the humerotriceps muscles based on preliminary experimental data. We used a set stimulus pulse duration of 0.2 ms and pulse frequency of 300 s^{-1}. The number of stimulus pulses per train varied depending on the stimulus duty cycle duration (% cycle) and on the length-change cycle frequency. Every work loop trial, including the control, contained six cycles per trial, regardless of the treatment.

Inspection of the raw sonomicrometry data that were graciously provided by the authors of a previous study, where they measured *in vivo* fascicle strains from the pigeon humerotriceps (Robertson and Biewener, 2012), revealed that there exists some level of individual variation with respect to the shape of this muscle's strain profile. Matching the *in vivo* fascicle strain profile of the pigeon humerotriceps would be desirable, but our work loop control software did not have this ability. Although the trajectory of the

in vivo fascicle strain profiles differed, they still retained a near-sinusoidal shape. Therefore, during our work loop experiments the strain profile was approximated by a sine wave.

Prior to analysis, we performed several validity checks of the humerotriceps work loop data using custom scripts written in MATLAB (R2016b, MathWorks Inc., Natick, MA, USA). First, we visually examined the EMG, length and force traces of each individual work loop trial to check for anomalies that could result from knot slippage, muscle tearing, servomotor malfunction, or loss of action potential propagation in the muscle. These anomalies would manifest as deviations from a sine wave for the length trace, unexplained changes in force or a substantial decrease in EMG signal amplitude, for example. We next visually inspected the third to fifth work loops in each trial to ensure that none of the work loops from an individual, for a given phase treatment, differed substantially from one another.

Finally, we examined the peak forces produced during the control work loops, which were run before and after each treatment. Since the net work and power output of the control work loops were not always positive, we chose to compare the means of peak forces of each control work loop to determine whether a given treatment should be included in the final dataset. We set a limit for force degradation based on the control work loop. Treatments were included if the control work loop that was tested just following a treatment had ≥59% of the peak force of the initial control work loop. We did not apply a correction to muscle force data based on degradation, but instead included degradation value in the statistical analysis.

We used 59% peak force as the cut-off because nearly all treatment sequences below this value exhibited one or both of the following problems: (1) notable departure of work loop shape from those typically observed for a given treatment, commonly through horizontal flattening of the loops or through marked decrease in area within each loop; (2) a substantial decrease (by close to half) in absolute power output at several, if not all of the phases. Two treatment sequences that were well below the 59% cut-off did not exhibit either problem but were excluded for consistency.

To further justify our decision to set the force degradation cut-off at ≥59%, we performed two sensitivity analyses on the work loop data, which demonstrated that the conclusions of the study were unaffected by this force degradation cut-off. We first reanalyzed our data using a more restrictive (higher) force degradation cut-off of ≥70%, relative to the control work loop (see Ellerby and Askew, 2007a). The 8.6 s^{-1} and 69% stimulus duty cycle treatment had four trials above the more restrictive cut-off, whereas the 8.6 s^{-1} and 50% stimulus duty cycle treatment had one trial above the cut-off. The power output curves and the summary statistics of these trials are plotted in Fig. S2. Comparison with similar plots for the larger data set indicated that the same conclusions are reached for comparable treatments.

We next performed an analysis of work loop data with varying force degradation cut-offs for the same treatments, including lower values. For the 8.6 s^{-1} and 50% stimulus duty cycle treatment, we compared two trials, one with a force cut-off of 71% and the other with a force cut-off of 60% (Fig. S3A). For the 10.1 s^{-1} 50% stimulus duty cycle treatment, we compared three trials, with cut-offs of 64%, 60% and 59% (Fig. S3B). Visual inspection of the GAM fits of the data reveal that the magnitudes and locations of net power values (with respect to stimulus onset) are not influenced by the force degradation cut-off.

Net work was calculated from the force and length data and was multiplied by frequency to obtain net power output using custom MATLAB scripts, and mass specific values were determined in R (v3.3.2, R Development Core Team, 2016). We averaged power output across the third through fifth work loops within each trial for a given stimulus onset phase for consistency and because not all trials contained six complete work loop cycles. These three values were also consistent and included the maximum values within each of the first set of four complete work loop cycles.

Statistical analysis

Twitch kinetics data for developed force and relaxation durations were compared using a paired sample *t*-test to test for significance. Our measures of developed force and relaxation durations were from 10 to 90% of peak force, thus constituting 80% of the full durations. We approximated the full developed force and relaxation durations by linearly extrapolating their respective time intervals from 80 to 100%. This information was then used to predict the maximum contractile cycle frequency of the muscle and provide additional description of basic properties of the pigeon humerotriceps. However, it should be noted that this prediction will likely differ from the maximum contractile cycle frequency in a shortening cycle, because force can be enhanced by stretch (Askew and Marsh, 1998). Specifically, relaxation is more rapid when the muscle is allowed to shorten (Askew and Marsh, 1998).

To evaluate the sinusoidal quality and frequency of the *in vivo* fascicle strain profiles of the pigeon humerotriceps we used a fast Fourier transform (FFT) to determine the main component frequencies, and their respective power spectral density (PSD) for strain profiles from five birds. This evaluation was also performed on the *in situ* strain profiles that we used during our work loop experiments. For the *in vivo* fascicle strains, we determined PSD of the main component frequencies from the FFT amplitudes averaged across five trials for each bird. A given frequency was considered to contribute to the shape of the waveform if that frequency's PSD was greater than an arbitrarily selected threshold of 1.42×10^{-9} mm^2 s. If deemed to be a contributing frequency, then the PSD of all of that frequency's harmonics were included in the total harmonic PSD that we used to determine the percentage that each fundamental frequency contributes to overall waveform shape. We determined what percentage of each of component frequency contributed to shaping the strain profiles of each bird by using the ratio of the PSD of each component frequency to the total harmonic PSD. We then determined the weighted mean fundamental frequency from the component frequencies of the strain profiles from each bird. We used these fundamental frequencies to qualitatively assess the similarity of the *in vivo* strain profiles from each bird, to those of the mechanically generated strain profiles that were used during our *in situ* work loop experiments.

To examine the contributions of stimulus phase to changes in power output and consequently the potential *in vivo* function of the pigeon humerotriceps within a given stimulus duration or cycle frequency treatment, we analyzed the power output of the humerotriceps across the full range of stimulus phases by fitting these data with a linear mixed-effects model. We then used a likelihood ratio test to compare this model to a null model that excluded phase as an explanatory variable. This method allowed us to compare power output among the different stimulus phases within each treatment (Table S1), while taking into account that there were repeated measures and autocorrelation over the duration of an experiment.

We addressed our first and second questions of how stimulus duty cycle and of how cycle frequency affects the muscle power output and thus its potential role *in vivo* by fitting the data from each

Journal of Experimental Biology (2019) 222, jeb195578. doi:10.1242/jeb.195578

treatment within these two comparison groups with a generalized additive model (GAM). The GAMs were fit for the power output across the full range of stimulus phases and included a cyclic component to account for the inclusion of both −50 and 50% phase, which are effectively the same. These models provided visual and quantitative characterization of the changes in power output that occur across the different treatment groups. We used the individual fits of each model to derive four summary statistics that quantify changes in shape of the power output curve: (1) mean power over the full range of phases, (2) maximum and (3) minimum power output, and (4) the percentage of the full stimulus phase cycle over which positive power is produced, hereafter referred to as actuation percentage. It is important to note that the mean power output at −30% phase was determined from both the first and the last trials within a treatment because this stimulus phase protocol was used to check for degradation every work loop treatment. We used an analysis of variance (ANOVA) to compare each of the four summary statistics of a given treatment to those of all other treatments within each of the two comparison groups. All statistical analyses were performed using R (v3.3.2, R Development Core Team, 2016).

RESULTS

Muscle twitch kinetics

Isometric contractions provided measures of the twitch kinetics of the pigeon humerotriceps muscle (Fig. 2A). As is typical for skeletal muscle, the humerotriceps muscle takes significantly longer to relax than to develop force ($P \leq 0.0001$; Fig. 2B; Table 2).

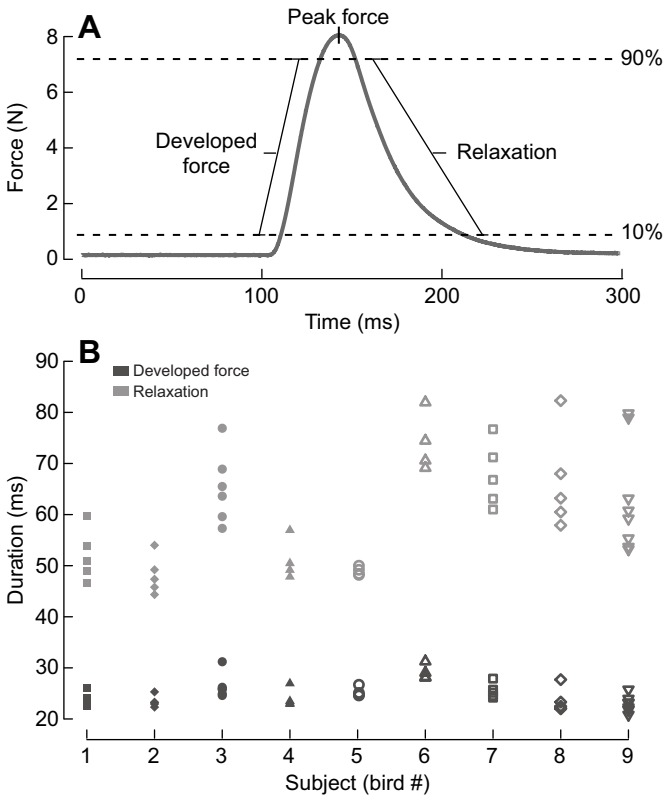

Fig. 2. Twitch kinetics of the pigeon humerotriceps muscle. (A) Sample two-pulse isometric contraction, with developed force (from 10 to 90% of peak force) shown on the ascending arm of the force trace and relaxation (from 90 to 10% of peak force) shown on the descending arm. (B) Developed force duration, from 10 to 90% peak force (dark gray), and relaxation duration, from 90 to 10% peak force (light gray). Each symbol represents a different individual subject (n=9). The mean developed force and relaxation durations differed significantly (P<0.0001).

Strain profile

We compared the *in vivo* and *in situ* strain profiles using an FFT analysis and the resultant weighted means of each strain profile's component frequencies (Fig. 3; see Table S2 for details). The comparison revealed a weighted mean fundamental frequency of 7.71 s^{-1} for the *in vivo* strain profiles from bird 1, 7.92 s^{-1} for bird 2, 7.57 s^{-1} for bird 3, 8.01 s^{-1} for bird 4 and 8.29 s^{-1} for bird 5 (Fig. 3B). These were close to the weighted mean fundamental frequency of 8.54 s^{-1} for the 8.6 s^{-1} *in situ* strain profile (Fig. 3B,C). The two extreme frequencies that we used had fundamental frequencies of 6.07 s^{-1}, and 10.1 s^{-1} for the 6.1 s^{-1} and 10.1 s^{-1} *in situ* strain profiles, respectively (Fig. 3C).

Work loop dynamics

The work loop technique provides measurements of how muscle force changes during the shortening–lengthening cycle, and further allows for other muscle performance measurements across the full cycle including maximum and minimum force, work, and power output. Representative results obtained through the *in situ* work loop technique are provided in Fig. 4. The time-dependent changes in stress (kPa), force (N) and muscle length (mm) are given for six consecutive length-change cycles of a single trial (Fig. 4A). In our experiments we covered the full suite of stimulus onset phases from −50 to 50% and because the sequence of length-change cycles always began and ended at −25%, trials where stimulus phases were earlier than this received incomplete stimulation in their first cycle. Conversely, trials where stimulus onset phase was 25% or later (depending on stimulus duration) received incomplete stimulation in the last cycle in a sequence. We therefore used six consecutive cycles because that accounted for changes in stimulus onset to ensure that at least four complete cycles were available for analysis. Plotting this data sequence as force and stress versus length for the four consistently complete cycles produces work loops (Fig. 4B). The area within each work loop is integrated to determine the net work output of each muscle contraction cycle (Fig. 4C). Absolute net work increases with cycle number but leveled off for the last three consistently complete work loops within a trial (Fig. 4C). The mean of these three cycles was therefore multiplied by frequency to determine the net power output of the humerotriceps muscle during each trial. Net power output values were then normalized using muscle mass.

The experiments were designed to examine the role of stimulus duty cycle and cycle frequency across the full range of stimulus onset phases. These work loop experiments quantified the changes in muscle work and power output with shifts in muscle activation timing at different activation durations, and contractile cycle frequencies (Figs 5 and 6). Across all of the treatments, work loops were primarily clockwise at nearly all of the stimulus onset phases, indicating work absorption and brake-like function (Fig. 5 and Fig. S4). However, as stimulus onset phase shifted from between −35 and −30% phase toward peak length (0% phase), work loops transitioned to counter-clockwise, indicating work production and actuator-like function (Fig. 5 and Fig. S2). Once stimulus phase surpassed peak length direction reversal was punctuated by work loops looping back on themselves such that they both produced and absorbed work and resembled a figure eight (Fig. 5). These figure eight-shaped loops had reduced force amplitude, indicating little to no net work or power output (Figs 5 and 6, respectively). Several of these stimulus phases yielded

Journal of Experimental Biology (2019) 222, jeb195578. doi:10.1242/jeb.195578

Table 2. Twitch kinetic data and estimates from two pulse isometric contractions in the pigeon humerotriceps

Subject (sample size)	Developed force duration (ms)	Relaxation duration (ms)	Estimated full developed force duration (ms)	Estimated full relaxation duration (ms)	Estimated full contractile cycle duration (ms)	Estimated max. frequency (s^{-1})
Bird 1 (*n*=5)	23.8±0.60	52.0±2.3	28.6±0.72	62.4±2.7	91.0±3.4	11.0±0.40
Bird 2 (*n*=5)	23.4±0.50	48.1±1.7	28.1±0.60	57.8±2.0	85.8±2.6	11.7±0.33
Bird 3 (*n*=6)	25.8±0.99	64.7±2.9	31.0±1.2	77.6±3.4	108.6±4.6	9.3±0.37
Bird 4 (*n*=4)	24.2±0.95	51.2±2.0	29.0±1.1	61.4±2.4	90.4±3.5	11.1±0.42
Bird 5 (*n*=4)	24.7±0.49	48.4±0.41	29.6±0.58	58.0±0.49	87.6±1.1	11.4±0.14
Bird 6 (*n*=4)	29.2±0.72	74.1±2.9	35.0±0.87	88.9±3.4	123.9±4.3	8.1±0.27
Bird 7 (*n*=5)	25.5±0.64	67.8±2.8	30.6±0.77	81.3±3.4	111.9±4.1	9.0±0.32
Bird 8 (*n*=5)	23.5±1.1	66.4±4.3	28.2±1.3	79.7±5.2	107.9±6.4	9.4±0.50
Bird 9 (*n*=8)	22.9±0.45	63.0±3.8	27.5±0.54	75.6±4.5	103.0±5.0	9.9±0.43
Mean of means:	24.8±0.64	59.5±3.2	29.7±0.77	71.4±3.9	101.1±4.4	10.1±0.42

All values are means±s.e.m. Developed force duration (from 10 to 90% of peak force), relaxation duration (from 90 to 10% of peak force). Estimates of full developed force duration (0 to 100% peak force), full relaxation duration (100% to 0% peak force), duration of a full contractile cycle and maximum contractile cycle frequency.

relatively steep work loops with reduced hysteresis, which were most prominent at the highest frequency, and provide evidence for high energy return that is characteristic of a spring (Fig. 5 and Fig. S2).

Variation in stimulus duty cycle, and in contractile cycle frequency both had modest effects on work loop shape. Increasing stimulus duration primarily caused a greater range of phases to exhibit spring-like function (Fig. 5B,C). Increasing frequency primarily caused a shift from low to higher stiffness, as indicated by the increase in work loop steepness (Fig. 5A,C,D).

Representative examples of work loops that indicate brake-like function (clockwise loops) occurred at 20% phase for all three frequencies, at 50% stimulus duty cycle (Fig. 5A,C,D). The best evidence for actuation occurred in work loops that were produced between −20% and 0% phase for 6.1 s^{-1}, and between −20% and −10% phase for 8.6 s^{-1}, both at 50% stimulus duty cycle (Fig. 5A,C). Work loops that exemplified relatively compliant spring-like function (loops with lower steepness reduced and hysteresis) occurred between 30 and 45% phase at 8.6 s^{-1} and 69% stimulus duty cycle (Fig. 5B), whereas work loops produced at these phases but at 10.1 s^{-1} and 50% stimulus duty cycle were steeper, providing evidence for stiffer spring-like function (Fig. 5D).

Effects of stimulus duty cycle on net muscle power output

We used the work loop technique to examine two different values for stimulus duty cycle (50% and 69% cycle) and tested each across the full range of stimulus phases to cover the high level of variability in the *in vivo* measurements of activation onset timing in flying pigeons. Stimulus onset phase had a significant effect on the net power output of the humerotriceps muscle, regardless of stimulus duty cycle (P<0.0001 for both stimulus duty cycles). Net muscle power output was also affected by stimulus duty cycle but both net power output curves retained similar shapes across the full range of stimulus onset phases. Moreover, the peak, trough and crossover regions of the net power output curves were similar.

The primary effect of reducing stimulus duty cycle from 69% to 50% was to increase the range of the humerotriceps net power output curve (Fig. 6B,C,E–G). The maximum net positive power output represents the most positive contractile work, whereas maximum net negative power output represents the most negative contractile work, and the lower stimulus duty cycle had the higher extrema (Fig. 6F). Although there was an increase in maximum net positive power as stimulus duration was decreased from 69% to 50% duty cycle (Fig. 6D), the difference between the two maxima was marginally insignificant (P=0.076). The maximum net negative power output did, however, show a significant increase when stimulus duty cycle was shifted from 69% to 50% (P=0.0034; Fig. 6F).

In addition to comparing the extrema of the net power output curves, comparison of the mean net power across all stimulus phases, and of the actuation percentages allowed us to further quantify any overall shifts in both the locality and the range of the net power output by phase curves between the two treatments (Fig. 6E and G, respectively). The mean net power output of the two treatments did not differ significantly across the full range of stimulus onset phases (P=0.559; Fig. 6E). The actuation percentage also did not differ among the two treatments (P=0.178; Fig. 6G).

Effects of contractile cycle frequency on net muscle power output

We tested three values of cycle frequency that represent the minimum, mean and maximum values determined from *in vivo* measurements of flying pigeons. As with the stimulus duty cycle treatments, each frequency was tested across the full range of stimulus phases. Cycle frequency affected humerotriceps net power production by increasing the overall range of the net power output curve with increasing frequency (Fig. 6A,C–G). Despite this increased range, net power produced by the humerotriceps was still increasingly negative as frequency increased (Fig. 6A,C–G).

The net power output by phase curves retained overall similarities in their shape, despite changes to the cycle frequency. This included the retention in location of the peak, trough and crossover regions. Varying stimulus onset phase had a significant effect on the net power output of the humerotriceps within each frequency treatment (P<0.0001 for all three frequencies).

Changes in the overall range of the power output curve among the three frequency treatments were again quantified through comparisons of extrema. As cycle frequency increased from 6.1 s^{-1} to 10.1 s^{-1}, there was a significant increase in the maximum net positive power output (P=0.0094; Fig. 6F). Increasing cycle frequency also caused a significant increase in maximum net negative power output (P<0.0001; Fig. 6F).

Shifts in location and range of the net power output curves across the three frequency treatments were again, further quantified by comparing the mean net power across the full suite of stimulus onset phases and the actuation percentages. Across the three frequency treatments, the mean net power output exhibited significant changes among the three frequencies (P<0.0001); mean net power output was lowest at 6.1 s^{-1}, and highest at 10.1 s^{-1} (Fig. 6E). The actuation percentages showed a significant decrease with increasing frequency (P=0.0068; Fig. 6G).

Journal of Experimental Biology (2019) 222, jeb195578. doi:10.1242/jeb.195578

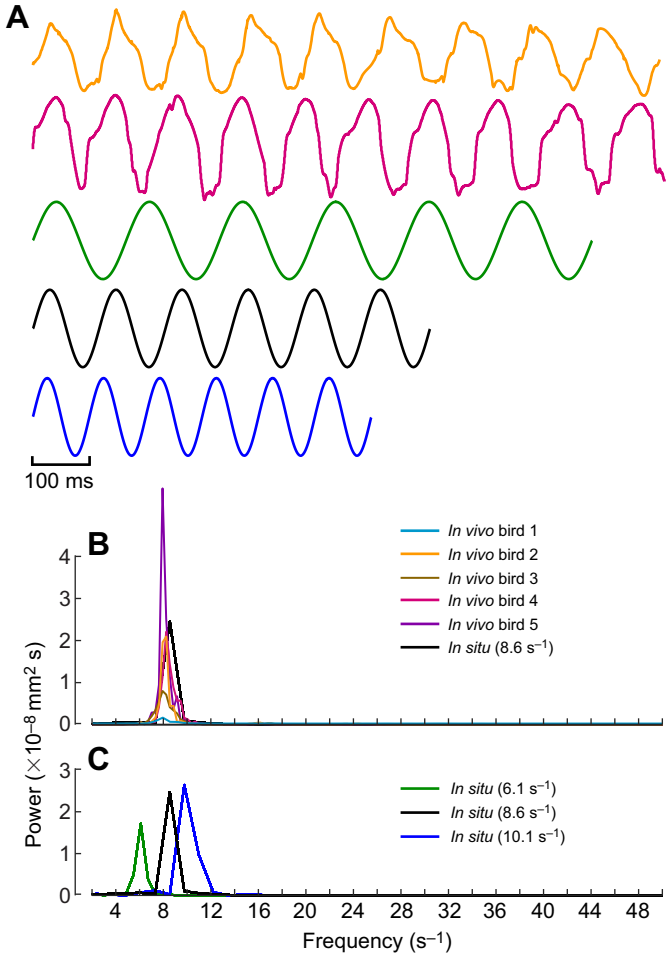

Fig. 3. Comparison of *in vivo* and *in situ* strain profiles for the pigeon humerotriceps. (A) Time course of fascicle strain measurements for two *in vivo* recordings (top two traces; refer to key in B) and representative *in situ* recordings (bottom three traces; see key in C) at the three cycle frequencies tested in this study. *In vivo* data are from sonomicrometry measurements in Robertson and Biewener (2012). *In situ* data were measured directly from the motor arm during work loop experiments. (B) Power spectral density (PSD; mm^2 s) from the fast Fourier transform (FFT) amplitudes averaged across five flights per bird for *in vivo* recordings from five birds [1: 7.7 s^{-1} (light blue); 2: 7.9 s^{-1} (orange); 3: 7.6 s^{-1} (brown); 4: 8.0 s^{-1} (pink); 5: 8.3 s^{-1} (violet)] are plotted with the PSD from the FFT of the *in situ* strains from the 8.6 s^{-1} cycle frequency treatments (black). (C) PSD from the FFT of the *in situ* strains from all three of the contractile cycle frequencies tested (6.1 s^{-1}, green; 8.6 s^{-1}, black; 10.1 s^{-1}, blue).

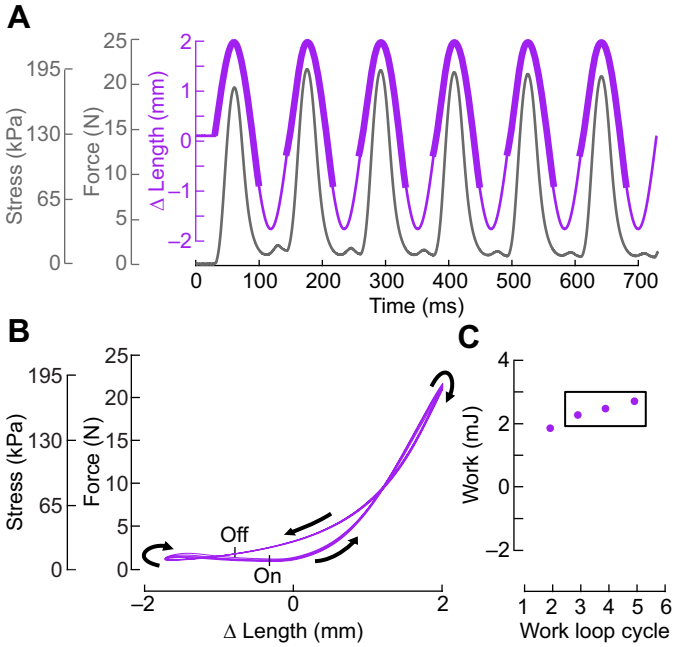

Fig. 4. Muscle force and length change from a work loop recording of the pigeon humerotriceps muscle. (A) The force (gray) and length (purple) are plotted as a function of time, with the scale for stress also provided for reference. Thick bands on the length trace indicate the period of applied stimulus to the nerve. (B) The resultant work loop traces are plotted as force versus length change, with the stress scale provided for reference. Arrows depict the direction of the loops, and counter-clockwise loop directionality indicates that the net work is positive. Work loops 2 through 5 are shown because varying stimulus onset phase caused either the first or the last of the six work loop cycles to receive incomplete muscle stimulation, and these four cycles were consistently complete. The start and end of the stimulus period are indicated by 'on' and 'off' marks, respectively. (C) The net work output from work loop cycles 2 to 5 within a trial is determined from the integrated area within each loop. The net work from the first and last loops is not shown. The box indicates the three work loops within a trial whose mean net work was used to calculate net power for the trial. The specific strain and stimulus parameters used in this recording were used for all control work loop trials. All control work loops were run at a cycle frequency of 8.6 s^{-1}, a stimulus onset phase of –30% cycle, and a stimulus duty cycle of 69%. The control work loop trials were run in between experimental treatment sequences to check the force degradation.

DISCUSSION

The muscles intrinsic to the avian wing are hypothesized to control wing morphing, but the specific functions of these muscles are uncertain because there have been no previous measurements of force dynamics. Wingbeat frequency, and *in vivo* activation and fascicle strain measurements are available for the humerotriceps muscle of pigeons (Dial, 1992b; Robertson and Biewener, 2012). Here, we adapted the *in situ* work loop technique (Nelson et al., 2004; Roberts and Azizi, 2010) to explore how natural variation in cycle frequency and muscle activation features affected its potential roles (Fig. 1). The *in situ* work loops varied in shape and direction, and across the *in vivo* ranges of stimulus phases, the humerotriceps muscle transitioned in the degree to which it functioned as an actuator, brake and spring (Fig. 5, Fig. S4). Variation in cycle frequency and stimulus duration had modest effects on the magnitude of muscle function, which was reflected through gradual changes in power output (Fig. 6). The overall high level of functional variation was observed within the ranges of *in vivo* parameters, which suggest that across even a small number of distinct flight modes, pigeons can radically alter the role of the humerotriceps.

In addition to the *in vivo* fascicle strain profile from the pigeon humerotriceps displayed in Robertson and Biewener (2012), the authors generously shared additional strain profiles from the same study. This included 25 fascicle strain profiles, five from each of five birds. The shortening-to-lengthening ratio was highly variable among these *in vivo* measures, with the shortening phase occupying as much as 61% or as little as 41% of the contractile cycle. Our experimental setup allowed for 50:50 shortening-to-lengthening phase ratio in a pure sine wave for the strain of the complete muscle-tendon unit. Comparison of the fast Fourier transforms of the *in vivo* fascicle strains and the *in situ* muscle-tendon sine wave strain at 8.6 s^{-1} indicates that almost all variation in the temporal domain is accounted for by the primary oscillation frequency (Fig. 3). Differences in the shortening-to-lengthening ratio may have had a

Journal of Experimental Biology (2019) 222, jeb195578. doi:10.1242/jeb.195578

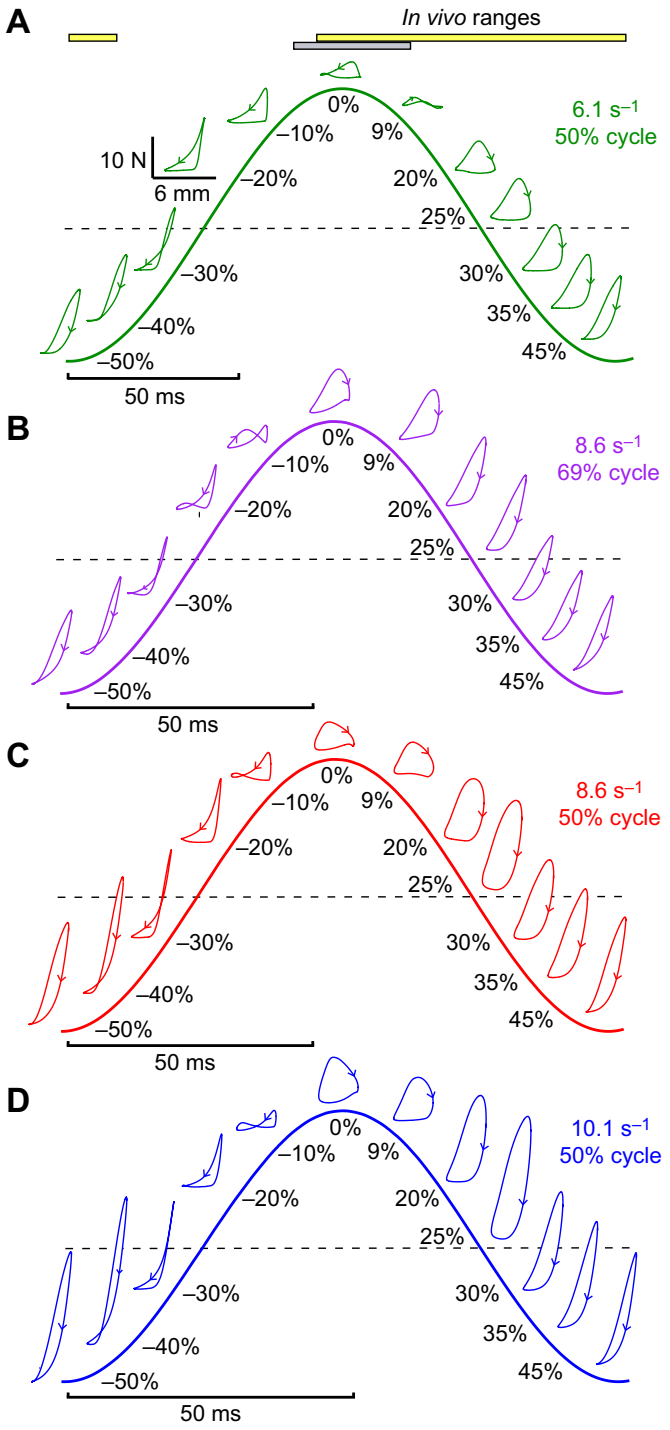

Fig. 5. Work loop shape changes substantially with stimulus onset phase, and modestly with changes in cycle frequency and stimulus duty cycle. (A) 6.1 s^{-1} and 50% stimulus duty cycle from bird 1 (green; *n*=2). (B) 8.6 s^{-1} and 69% stimulus duty cycle from bird 1 (purple; *n*=4 for all phases except –45, 0, 15 and 40%; *n*=3). (C) 8.6 s^{-1} and 50% stimulus duty cycle from bird 6 (red; *n*=2). (D) 10.1 s^{-1} and 50% stimulus duty cycle from bird 8 (blue; *n*=3). Representative work loops from the suite of stimulus onset phases are shown for all four treatments and are as follows: –50, –40, –30, –20, –10, 0, 9, 20, 25, 30, 35 and 45% phase. All work loops are the fourth loop from each trial and are plotted on the same scale: absolute length change and force are shown at –20% stimulus phase (A; horizontal and vertical bars, respectively). The *in vivo* ranges of phases recorded by Dial (1992b), and Robertson and Biewener (2012) are highlighted (A; horizontal yellow and gray bars, respectively).

more substantial effect on our interpretation of the muscle's potential functions. The twitch kinetics that we measured from the pigeon humerotriceps demonstrate that force development duration was less than half that of its relaxation duration (Fig. 2). When this kinetic result is coupled with the highly variable *in vivo* shortening-to-lengthening ratio, it becomes evident that at key activation phases, the *in vivo* strain profile could generate substantially different contractile forces than for equivalent *in situ* measurements. For example, strain profiles with longer shortening periods would have increased net work and power output (Askew and Marsh, 1997; Ellerby and Askew, 2007a,b; Josephson, 1993; Sawicki et al., 2015). These strain profiles would likely result in more phases that exhibit the capacity for actuation. By contrast, strain profiles with longer lengthening periods would have decreased net work and power output (Askew and Marsh, 1997; Ellerby and Askew, 2007a,b; Josephson, 1993; Sawicki et al., 2015). These strain profiles would likely result in more phases exhibiting spring- or brake-like functions. Thus, the *in situ* setup may have limited the humerotriceps muscle's net work and power output by restricting its shortening-to-lengthening phase ratio (Askew and Marsh, 1997; Ellerby and Askew, 2007a,b; Josephson, 1993; Sawicki et al., 2015).

During flapping flight, it has previously been hypothesized that birds use their humerotriceps muscles to fill two roles: (1) to actuate elbow extension and wing expansion; (2) to stabilize the elbow joint angle, smoothing the transition from the upstroke to the downstroke (Dial, 1992b; Robertson and Biewener, 2012). It is possible to evaluate if these roles are fulfilled by plotting the instantaneous power through the stroke cycle, for key activation phases within the *in vivo* ranges. Overall, the instantaneous power that is produced by the pigeon humerotriceps through the stroke cycle provides support for both of these hypotheses for the role of this muscle (Fig. 7).

The activation duration of the pigeon's humerotriceps muscle is relatively long, causing it to have substantial positive and negative work, and positive and negative instantaneous power. Moreover, this attribute occurred consistently across all of the stimulus duration and cycle frequency treatments within the *in vivo* ranges of activation onset phases (Fig. 7). We observed transitions between positive and negative work (and power) in a single contractile cycle that had steep work loops with reduced hysteresis and low net work. The portion of one wingbeat or contractile cycle over which positive instantaneous power is produced by the humerotriceps muscle suggests that it is serving as an actuator by contributing energy towards elbow extension and wing expansion (Fig. 7). The portion of a contractile cycle over which negative instantaneous power is produced by the humerotriceps muscle suggests that it is serving to stabilize the elbow by resisting wing folding that is caused by aerodynamic forces. It also suggests that the muscle can act as a brake by absorbing energy that is likely contributed by the biceps to fold the wing, effectively slowing wing folding and helping smooth the transition from the upstroke to the downstroke. Negative instantaneous power suggests that the muscle is serving as a brake and resisting elbow flexion during that particular portion of its contractile cycle. In most cases, the muscle primarily produced negative instantaneous power over the course of one cycle (Fig. 7), which implies that stabilization of the elbow joint and resistance to wing folding likely requires more work than does elbow extension and wing expansion. Collectively, these results suggest that the muscle is able to fulfill both actuation and stabilization within a single contractile cycle, by having an extended stimulation duty cycle.

Multifunctional roles within a cycle have previously been demonstrated during terrestrial locomotion including in hopping tammar wallabies (*Macropus eugenii*) (Biewener et al., 1998b) and

Journal of Experimental Biology (2019) 222, jeb195578. doi:10.1242/jeb.195578

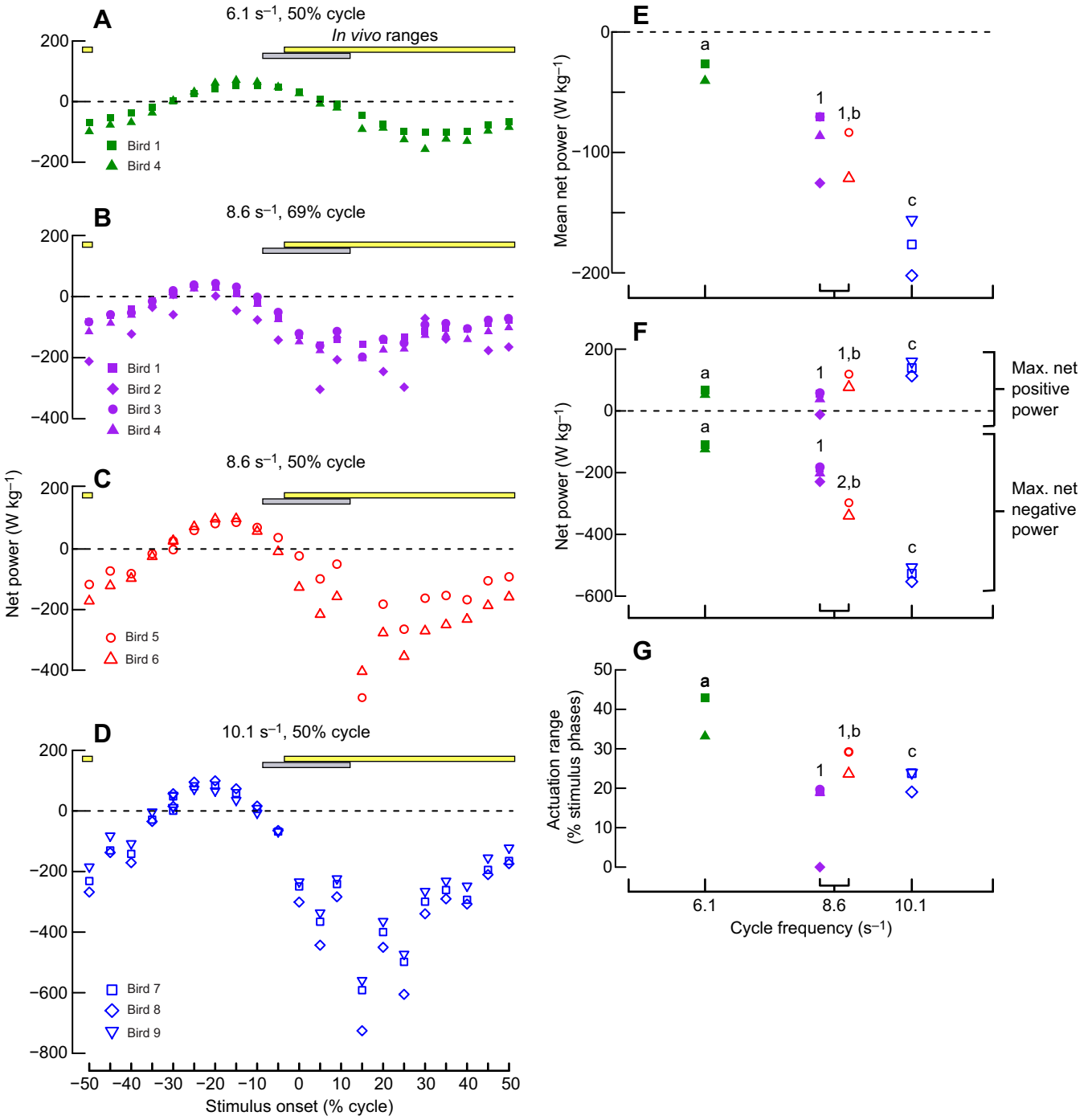

Fig. 6. Net power output from the pigeon humerotriceps shifts as a result of changes in stimulus onset phase, stimulus duty cycle and cycle frequency. (A–D) Net power output of the humerotriceps muscle across the full stimulus phase cycle (−50 to 50%) was tested at two stimulus duty cycles for 8.6 s^{-1} and three cycle frequencies, for a total of four treatments (experimental parameters, sample sizes, colors and the *in vivo* ranges of phases as in Fig. 5). Symbols for individual birds as in Fig. 2. (E–G) Summary statistics determined from the individual fits of the generalized additive model. (E) The mean net power output across the full range of phases (−50 to 50%) within a treatment sequence. (F) The range of net power denoted using the maximum net positive and maximum net negative power produced by the humerotriceps. (G) The percentage of stimulus onset phases over which the net power output is positive. Net power output by stimulus phase response curves of all treatments had a slope that differed significantly from zero (P<0.05). Letters indicate significant differences (P<0.05) among frequency treatments. Numbers indicate significant differences (P<0.05) between the two stimulus duty cycle treatments, both tested at 8.6 s^{-1}. Horizontal yellow and gray bars as described in Fig. 5.

running turkeys (*Meleagris gallopavo*) (Gabaldón et al., 2004). Thus, during hopping, running and now flying, there is evidence for functional shifts over the course of one contractile cycle, where the muscles serve as stabilizers or brakes during one portion and propulsors or actuators during another.

The relative contributions of positive and negative power within a cycle will be determined in part by activation onset phase. Several *in vivo* studies provide evidence that pigeons shift activation onset phase of the humerotriceps as a function of flight mode (Dial, 1992b; Robertson and Biewener, 2012; see also Table 1). For

Journal of Experimental Biology (2019) 222, jeb195578. doi:10.1242/jeb.195578

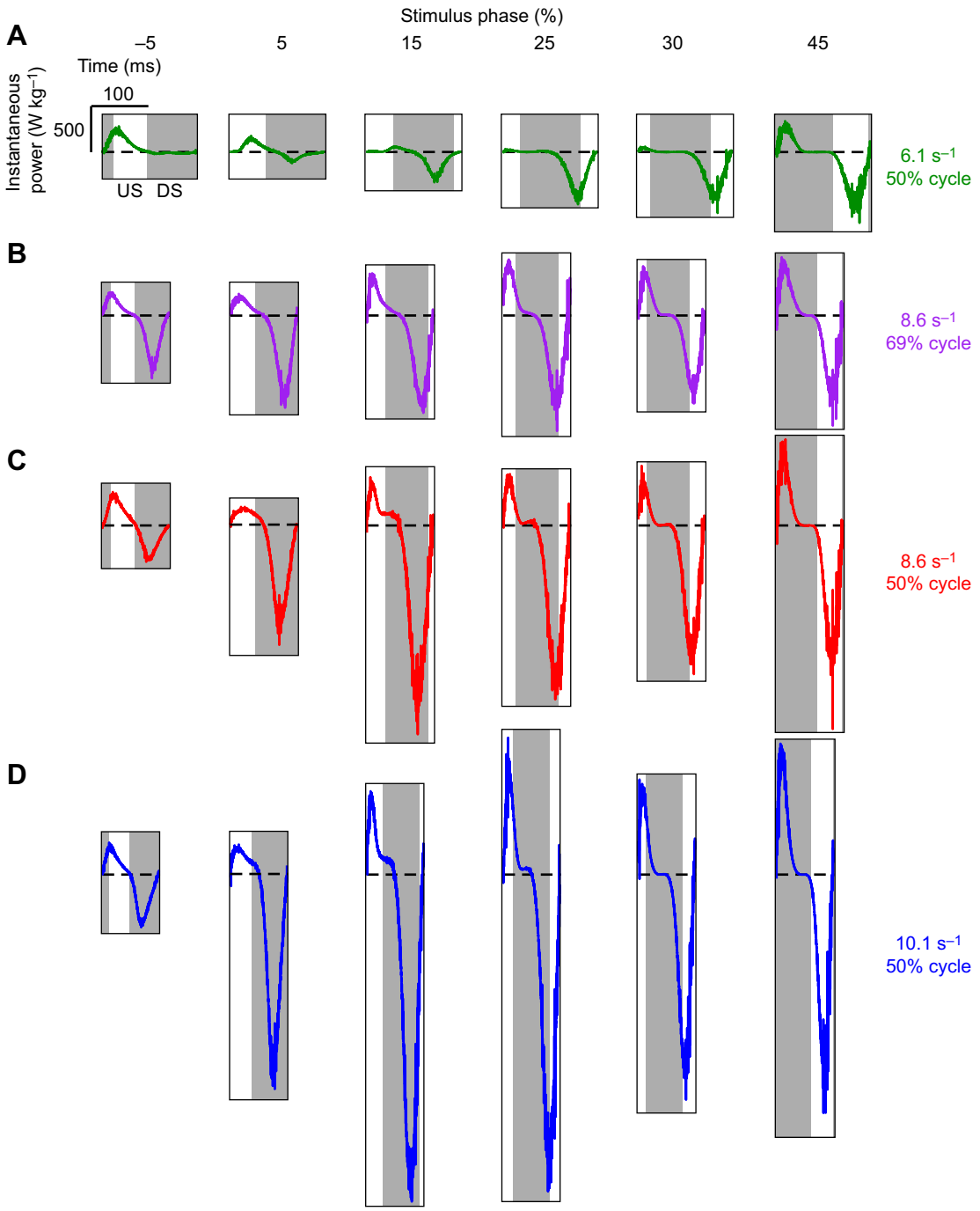

Fig. 7. Instantaneous power from the pigeon humerotriceps. (A–D) Instantaneous power output from representative individuals for each of the four different treatments used for this study plotted over time for six out of the 22 stimulus onset phases, which highlight key phases within the *in vivo* ranges of activation onsets. Individuals used for plotting, experimental parameters, sample sizes, and colors as in Fig. 5. All instantaneous power plots are from the fourth loop from each trial and are plotted on the same scale: instantaneous power and time are shown at –5% stimulus phase (A; vertical and horizontal bars, respectively). US and DS (A) denote the up- and down-stroke (white and gray bars, respectively), with wingbeat cycle percentages and ratios taken as the grand means that were measured by Robertson and Biewener (2012).

example, with an early activation onset at the average wingbeat frequency (8.6 s^{-1}) that might be observed during level flight, peak positive power occurs at the transition from the downstroke to the upstroke, suggesting that the humerotriceps is being used to maintain elbow extension through to the end of the downstroke. During the downstroke itself, the muscle produces negative power, suggesting that it is being used to resist elbow flexion and stabilize the joint (see Table 1 and first panels of Fig. 7B,C). In contrast, with a later activation onset, and higher wingbeat frequency (10.1 s^{-1}) that might be observed during takeoff, the positive and negative components of instantaneous power would be shifted. Peak positive power would coincide with the upstroke to downstroke transition, and peak negative power would coincide with the downstroke to upstroke transition (see Table 1 and the three rightmost panels of Fig. 7D). In this case, the former would suggest that the muscle is being used to help initiate elbow extension rather than maintain it,

and the latter would again suggest resistance to elbow flexion and contributions to joint stability.

Shifting activation onset phase to generate different muscle functions has previously been demonstrated in terrestrial locomotion. Sawicki and colleagues (2015) found that in the plantaris of bullfrogs (*Lithobates catesbeianus*), shifting the onset of muscle activation produced a sinusoidal power output by onset phase response curve, indicating that this shift effectively allows the bullfrog's plantaris to transition from actuator to spring to brake. Interestingly, they also noted it was difficult to generate strut-like behavior through changes in activation phase alone, as contractions exhibited both positive and negative work components (Sawicki et al., 2015), much like we observed in our study (Fig. 7). Ahn and Full (2002) noted that in two seemingly redundant leg muscles (177c and 179) of cockroaches (*Blaberus discoidalis*), activation onset phase contributes to functional differences among these two muscles during running. Under *in vivo* conditions, muscle 177c is activated slightly later relative to its length-change cycle than muscle 179 such that the former always produces positive power and the latter always produces negative power. This type of functional modulation has also been documented in the peroneus longus muscles of wild turkeys. The timing of peak force can be shifted such that during downhill running, it occurs early in the stance phase allowing this muscle to produce negative work, whereas during uphill running it occurs late in the stance phase to produce positive work (Gabaldón et al., 2004).

Although the results of our study provide clues as to how pigeons use their humerotriceps muscles during certain flight modes, it is worth drawing attention back to the anatomical complexity of the intrinsic wing musculature. There are likely co-contracting synergistic and antagonistic muscles whose contributions need to be taken into account when determining *in vivo* muscle function. Therefore, we acknowledge that the function of the pigeon humerotriceps may not be as clear cut as what is presented here.

An additional mechanism that has the potential to shift functional roles of a muscle is to vary the shortening-to-lengthening ratio. Highly asymmetrical strains are commonly observed in isolated, ballistic movements such as leaping in anurans (Ahn et al., 2003; Gillis and Biewener, 2000; Olson and Marsh, 1998), vertical jumping in cats (Abraham and Loeb, 1985) and fast starts in fish (Ellerby and Altringham, 2001; Goldbogen et al., 2005; James and Johnston, 1998; Wakeling and Johnston, 1999). Cyclic movements are constrained to have more symmetrical shortening and lengthening (Girgenrath and Marsh, 1997). However, deviations from symmetry have been observed in nearly all previous measurements from level flight (Biewener et al., 1998a; Ellerby and Askew, 2007b; Hedrick et al., 2003; Robertson and Biewener, 2012; Tobalske and Biewener, 2008; Williamson et al., 2001). The shortening phase of the pectoralis major, which powers the downstroke, is typically upwards of 60% during low- or high-speed level flight (Biewener et al., 1998a; Ellerby and Askew, 2007b; Hedrick et al., 2003; Tobalske and Biewener, 2008; Williamson et al., 2001), which has the potential to enhance the positive power (Biewener et al., 1998a; Ellerby and Askew, 2007a, b). The shortening-to-lengthening ratio from the *in vivo* fascicle strain measurements of the pigeon humerotriceps can vary substantially, ranging from 41:59 to 61:39. It is unknown how these fascicle strain ratios translate to whole muscle–tendon unit shortening-to-lengthening ratios. However, these results are highly suggestive that pigeons may be varying shortening-to-lengthening ratio to further modify muscle function. This hypothesis could be tested using *in vivo* strain profiles from the muscle–tendon unit in an *in situ* experiment with the capacity for asymmetrical strain trajectories.

Acknowledgements
We thank L. Kolody and K. Morden for assistance with surgical procedures and experiments. M. S, Armstrong, V. B. Baliga, R. Dakin, A. H. Gaede, C. Harvey, P. G. D. Matthews, W. K. Milsom, D. A. Skandalis, D. Schluter, G. C. Smyth, D. A. Syme and J. Wong provided helpful suggestions and edits.

Competing interests
The authors declare no competing or financial interests.

Author contributions
Conceptualization: J.S.T., J.W.B., R.E.S., D.L.A.; Methodology: J.S.T., J.W.B.; Software: J.S.T., J.W.B.; Investigation: J.S.T.; Data curation: J.S.T.; Writing - original draft: J.S.T., D.L.A.; Writing - review & editing: J.S.T., J.W.B., R.E.S., D.L.A.; Visualization: J.S.T.; Supervision: D.L.A.; Funding acquisition: D.L.A.

Funding
The research was funded by the U.S. Air Force Office of Scientific Research, grant number FA9550-16-1-0182, monitored by Dr B. L. Lee, and by the Natural Sciences and Engineering Research Council of Canada (NSERC, RGPIN-2016-05381). J.S.T. was also supported by an NSERC Canada Graduate Scholarship.

Data availability
All data and scripts are available through Figshare at dx.doi.org/10.6084/m9.figshare.7336085.

Supplementary information
Supplementary information available online at http://jeb.biologists.org/lookup/doi/10.1242/jeb.195578.supplemental

References
Abraham, L. D. and Loeb, G. E. (1985). The distal hindlimb musculature of the cat. *Exp. Brain Res.* **58**, 580-593. doi:10.1007/BF00235874

Ahn, A. N. and Full, R. J. (2002). A motor and a brake: two leg extensor muscles acting at the same joint manage energy differently in a running insect. *J. Exp. Biol.* **205**, 379-389.

Ahn, A. N., Monti, R. J. and Biewener, A. A. (2003). *In vivo* and *in vitro* heterogeneity of segment length changes in the semimembranosus muscle of the toad. *J. Physiol.* **549**, 877-888. doi:10.1113/jphysiol.2002.038018

Altshuler, D. L., Bahlman, J. W., Dakin, R., Gaede, A. H., Goller, B., Lentink, D., Segre, P. S. and Skandalis, D. A. (2015). The biophysics of bird flight: functional relationships integrate aerodynamics, morphology, kinematics, muscles, and sensors. *Can. J. Zool.* **93**, 961-975. doi:10.1139/cjz-2015-0103

Askew, G. N. and Marsh, R. L. (1997). The effects of length trajectory on the mechanical power output of mouse skeletal muscles. *J. Exp. Biol.* **200**, 3119-3131.

Askew, G. N. and Marsh, R. L. (1998). Optimal shortening velocity (V/V_{max}) of skeletal muscle during cyclical contractions: length-force effects and velocity-dependent activation and deactivation. *J. Exp. Biol.* **201**, 1527-1540.

Berg, A. M. and Biewener, A. A. (2008). Kinematics and power requirements of ascending and descending flight in the pigeon (*Columba livia*). *J. Exp. Biol.* **211**, 1120-1130. doi:10.1242/jeb.010413

Berg, A. M. and Biewener, A. A. (2010). Wing and body kinematics of takeoff and landing flight in the pigeon (*Columba livia*). *J. Exp. Biol.* **213**, 1651-1658. doi:10.1242/jeb.038109

Biewener, A. A., Corning, W. R. and Tobalske, B. W. (1998a). *In vivo* pectoralis muscle force-length behavior during level flight in pigeons (*Columba livia*). *J. Exp. Biol.* **201**, 3293-3307.

Biewener, A. A., Konieczynski, D. D. and Baudinette, R. V. (1998b). *In vivo* muscle force-length behavior during steady-speed hopping in tammar wallabies. *J. Exp. Biol.* **201**, 1681-1694.

Chatterjee, S. (2015). *The Rise of Birds: 225 Years of Evolution*, 2nd edn. Baltimore: Johns Hopkins University Press.

Chin, D. D., Matloff, L. Y., Stowers, A. K., Tucci, E. R. and Lentink, D. (2017). Inspiration for wing design: how forelimb specialization enables active flight in modern vertebrates. *J. R. Soc. Interface* **14**, 20170240. doi:10.1098/rsif.2017.0240

Dial, K. P. (1992a). Avian forelimb muscles and nonsteady flight: can birds fly without using the muscles in their wings? *Auk* **109**, 874-885. doi:10.2307/4088162

Dial, K. P. (1992b). Activity patterns of the wing muscles of the pigeon (*Columba livia*) during different modes of flight. *J. Exp. Zool.* **262**, 357-373. doi:10.1002/jez.1402620402

Dial, K. P., Goslow, G. E. and Jenkins, F. A. (1991). The functional anatomy of the shoulder in the European starling (*Sturnus vulgaris*). *J. Morphol.* **207**, 327-344. doi:10.1002/jmor.1052070309

Dickinson, M. H., Farley, C. T., Full, R. J., Koehl, M. A. R., Kram, R. and Lehman, S. (2000). How animals move: an integrative view. *Science* **288**, 100-106. doi:10.1126/science.288.5463.100

Ellerby, D. J. and Altringham, J. D. (2001). Spatial variation in fast muscle function of the rainbow trout *Oncorhynchus mykiss* during fast-starts and sprinting. *J. Exp. Biol.* **204**, 2239-2250.

Ellerby, D. J. and Askew, G. N. (2007a). Modulation of flight muscle power output in budgerigars *Melopsittacus undulatus* and zebra finches *Taeniopygia guttata*: *in vitro* muscle performance. *J. Exp. Biol.* **210**, 3780-3788. doi:10.1242/jeb.006288

Ellerby, D. J. and Askew, G. N. (2007b). Modulation of pectoralis muscle function in budgerigars *Melopsittacus undulatus* and zebra finches *Taeniopygia guttata* in response to changing flight speed. *J. Exp. Biol.* **210**, 3789-3797. doi:10.1242/jeb.006296

Gabaldón, A. M., Nelson, F. E. and Roberts, T. J. (2004). Mechanical function of two ankle extensors in wild turkeys: shifts from energy production to energy absorption during incline versus decline running. *J. Exp. Biol.* **207**, 2277-2288. doi:10.1242/jeb.01006

Gillis, G. B. and Biewener, A. A. (2000). Hindlimb extensor muscle function during jumping and swimming in the toad (*Bufo marinus*). *J. Exp. Biol.* **203**, 3547-3563.

Girgenrath, M. and Marsh, R. L. (1997). *In vivo* performance of trunk muscles in tree frogs during calling. *J. Exp. Biol.* **200**, 3101-3108.

Goldbogen, J. A., Shadwick, R. E., Fudge, D. S. and Gosline, J. M. (2005). Fast-start muscle dynamics in the rainbow trout *Oncorhynchus mykiss*: phase relationship of white muscle shortening and body curvature. *J. Exp. Biol.* **208**, 929-938. doi:10.1242/jeb.01433

Hedrick, T. L., Tobalske, B. W. and Biewener, A. A. (2003). How cockatiels (*Nymphicus hollandicus*) modulate pectoralis power output across flight speeds. *J. Exp. Biol.* **206**, 1363-1378. doi:10.1242/jeb.00272

James, R. S. and Johnston, I. A. (1998). Scaling of muscle performance during escape responses in the fish *Myoxocephalus scorpius* L. *J. Exp. Biol.* **201**, 913-923.

Josephson, R. K. (1985). Mechanical power output from striated muscle during cyclic contraction. *J. Exp. Biol.* **114**, 493-512.

Josephson, R. K. (1993). Contraction dynamics and power output of skeletal muscle. *Annu. Rev. Physiol.* **55**, 527-546. doi:10.1146/annurev.ph.55.030193.002523

Josephson, R. K. (1997). Power output from a flight muscle of the bumblebee *Bombus terrestris*. *J. Exp. Biol.* **1246**, 1241-1246.

King, A. S. and McLelland, J. (1984). Nervous system. In *Birds: Their Structure and Function*, pp. 266-269. East Sussex: Baillière Tindall.

Konow, N., Cheney, J. A., Roberts, T. J., Waldman, J. R. S. and Swartz, S. M. (2015). Spring or string: does tendon elastic action influence wing muscle mechanics in bat flight? *Proc. R. Soc. B Biol. Sci.* **282**, 1-7. doi:10.1098/rspb.2015.1832

Lacourpaille, L., Nordez, A. and Hug, F. (2013). Influence of stimulus intensity on electromechanical delay and its mechanisms. *J. Electromyogr. Kinesiol.* **23**, 51-55. doi:10.1016/j.jelekin.2012.06.010

Lentink, D., Müller, U. K., Stamhuis, E. J., De Kat, R., Van Gestel, W., Veldhuis, L. L. M., Henningsson, P., Hedenström, A., Videler, J. J. and Van Leeuwen, J. L. (2007). How swifts control their glide performance with morphing wings. *Nature* **446**, 1082-1085. doi:10.1038/nature05733

Nelson, F. E., Gabaldón, A. M. and Roberts, T. J. (2004). Force-velocity properties of two avian hindlimb muscles. *Comp. Biochem. Physiol. A Mol. Integr. Physiol.* **137**, 711-721. doi:10.1016/j.cbpb.2004.02.004

Olson, J. M. and Marsh, R. L. (1998). Activation patterns and length changes in hindlimb muscles of the bullfrog *Rana catesbeiana* during jumping. *J. Exp. Biol.* **201**, 2763-2777.

Pennycuick, C. J. (1968). A wind-tunnel study of gliding flight in the pigeon *Columba livia*. *J. Exp. Biol.* **49**, 509-526.

Pennycuick, C. J. (2015). The flight of birds and other animals. *Aerospace* **2**, 505-523. doi:10.3390/aerospace2030505

Roberts, T. J. and Azizi, E. (2010). The series-elastic shock absorber: tendons attenuate muscle power during eccentric actions. *J. Appl. Physiol.* **109**, 396-404. doi:10.1152/japplphysiol.01272.2009

Roberts, T. J., Marsh, R. L., Weyand, P. G. and Taylor, C. R. (1997). Muscular force in running turkeys: the economy of minimizing work. *Science* **275**, 1113-1115. doi:10.1126/science.275.5303.1113

Robertson, A. M. B. and Biewener, A. A. (2012). Muscle function during takeoff and landing flight in the pigeon (*Columba livia*). *J. Exp. Biol.* **215**, 4104-4114. doi:10.1242/jeb.075275

Sawicki, G. S., Robertson, B. D., Azizi, E. and Roberts, T. J. (2015). Timing matters: tuning the mechanics of a muscle-tendon unit by adjusting stimulation phase during cyclic contractions. *J. Exp. Biol.* **218**, 3150-3159. doi:10.1242/jeb.121673

Tobalske, B. W. (2007). Biomechanics of bird flight. *J. Exp. Biol.* **210**, 3135-3146. doi:10.1242/jeb.000273

Tobalske, B. W. and Biewener, A. A. (2008). Contractile properties of the pigeon supracoracoideus during different modes of flight. *J. Exp. Biol.* **211**, 170-179. doi:10.1242/jeb.007476

Usherwood, J. R., Stavrou, M., Lowe, J. C., Roskilly, K. and Wilson, A. M. (2011). Flying in a flock comes at a cost in pigeons. *Nature* **474**, 494-497. doi:10.1038/nature10164

Vazquez, R. J. (1994). The automating skeletal and muscular mechanisms of the avian wing (Aves). *Zoomorphology* **114**, 59-71. doi:10.1007/BF00574915

Wakeling, J. M. and Johnston, I. A. (1999). Body bending during fast-starts in fish can be explained in terms of muscle torque and hydrodynamic resistance. *J. Exp. Biol.* **202**, 675-682.

Williamson, M. R., Dial, K. P. and Biewener, A. A. (2001). Pectoralis muscle performance during ascending and slow level flight in mallards (*Anas platyrhynchos*). *J. Exp. Biol.* **204**, 495-507.

Table S1: Experimental treatments and work loop parameters.

Treatment	Cycle Frequency (s^{-1})	Stimulus duty cycle (%)	Stimulus onset phases (% cycle)	Birds	Sample size per treatment (n)
Stimulus phase and duty cycle	8.6	69	-50 to 5, 9, 15 to 50	1-4	4
Stimulus phase and cycle frequency	6.1	50	-50 to 5, 9, 15 to 50	1,4	2
Stimulus phase, duty cycle, and cycle frequency	8.6	50	-50 to 5, 9, 15 to 50	5,6	2
Stimulus phase and cycle frequency	10.1	50	-50 to 5, 9, 15 to 50	7-9	3

This study contained four different experimental treatments. Treatment indicates the work loop parameters that were varied. The subjects that they were measured from (Birds) and the total sample size per treatment (n) are also outlined. Stimulus onset phases were examined at the same intervals for all experimental treatments.

Journal of Experimental Biology • Supplementary information

Table S2. Comparison of *in vivo* and *in situ* strain profiles for the pigeon humerotriceps muscle with a Fast Fourier transform (FFT) analysis.

Strain profile	Component frequencies (s^{-1})	Contribution to waveform shape (%)	Weighted mean fundamental frequency (s^{-1})
In vivo Bird 1	7.93	97.2	7.71
In vivo Bird 2	8.24	36.6	7.92
	7.93	34.2	
	7.63	8.35	
	8.85	7.74	
	8.54	7.73	
	7.32	2.82	
In vivo Bird 3	7.93	20.7	7.57
	8.24	18.5	
	7.63	14.0	
	8.54	10.7	
	8.85	8.79	
	7.32	8.75	
	9.16	6.95	
	7.02	5.21	
In vivo Bird 4	7.93	46.8	8.01
	8.24	21.0	
	8.54	9.61	
	7.63	7.87	
	9.16	5.63	
	8.85	3.12	
	7.32	2.46	
	7.02	2.41	
In vivo Bird 5	8.24	29.2	8.29
	8.54	19.0	
	7.93	14.9	
	8.85	11.8	
	9.16	7.60	
	9.46	7.55	
	7.63	5.51	
	9.77	2.13	
8.6 s^{-1} *in situ*	8.54	100	8.54
6.1 s^{-1} *in situ*	6.10	66.0	6.07
	5.49	18.9	
	6.71	14.9	
10.1 s^{-1} *in situ*	9.76	73.0	10.1
	11.0	26.8	

Component frequencies of each strain profile were determined using a minimum threshold power spectral density (PSD) of 1.42×10^{-9} mm^2 s. The contribution of each component frequency is the percentage that each frequency contributed to the shape of the waveform, relative to the summed PSD from all of the component frequencies and their respective harmonic frequencies. The fundamental frequency of each strain profile was calculated using the weighted mean of all of its component frequencies.

Journal of Experimental Biology • Supplementary information

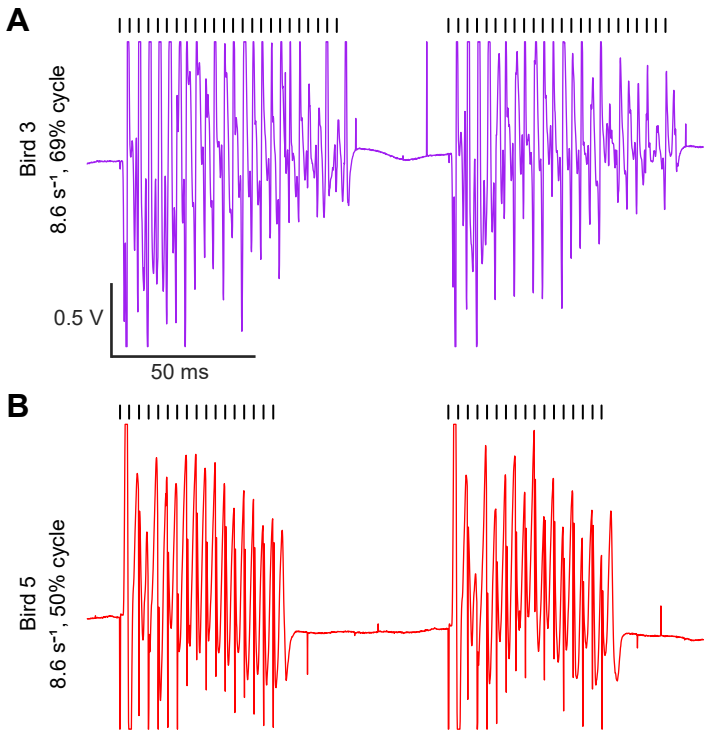

Fig. S1. Electromyogram recordings (EMGs) of evoked muscle potentials during work loop trials. Sample traces from raw EMG signals are plotted as voltage (V) over time (ms). Colours for each treatment as in Fig. 5. (A) EMG signal recorded during one work loop trial at -30% stimulus phase and 69% stimulus duty cycle from Bird 3. (B) EMG signal recorded during one work loop trial at 50% phase and 50% stimulus duty cycle from Bird 5. Both EMG traces were recorded from the fourth and fifth work loop cycles, at a frequency of 8.6 s^{-1}, and are plotted on the same scale, with scale bars included for both voltage and time (A; vertical and horizontal bars, respectively). Ticks above each EMG trace denote the applied stimulus timing (black). Stimulus intensities were set at 6mA, 60V for both experiments.

Journal of Experimental Biology • Supplementary information

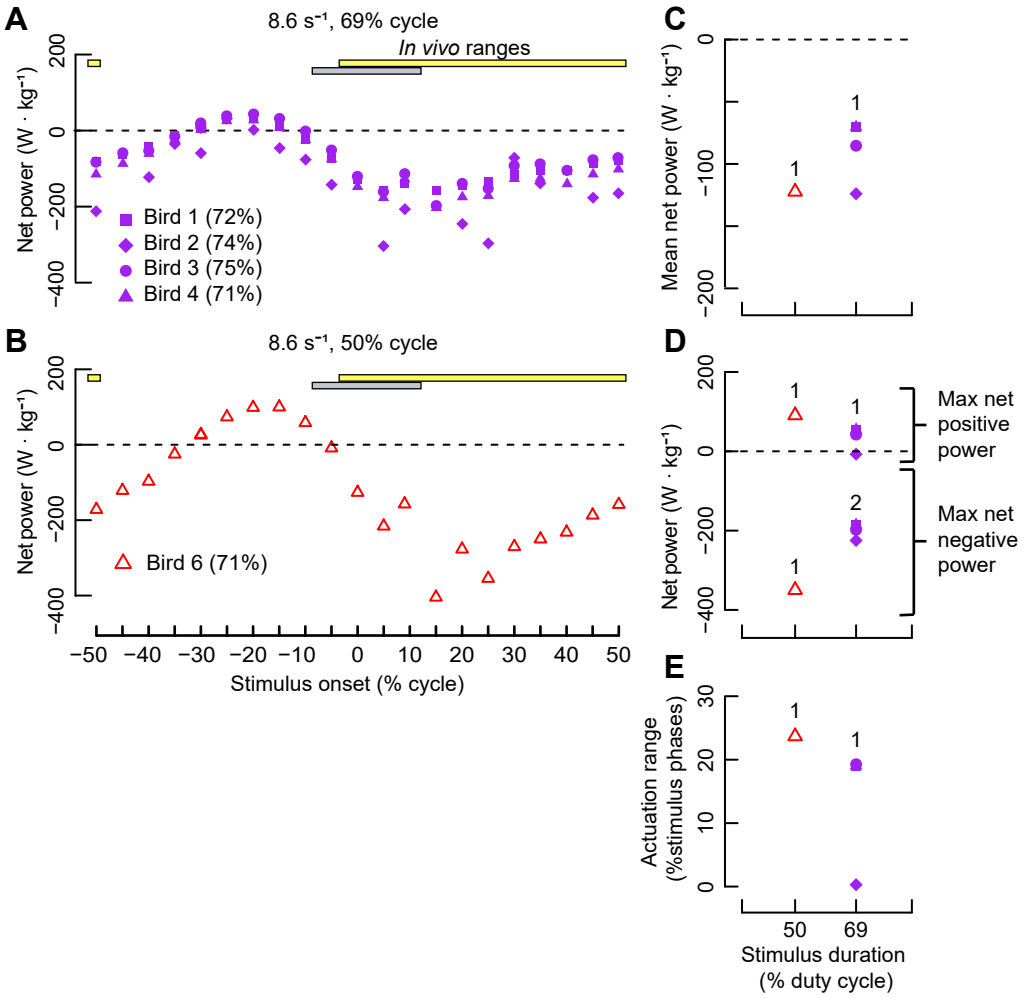

Fig. S2. The first sensitivity analysis indicates that raising the force degradation cut-off does not affect work loop results. Net power output of the humerotriceps muscle across the full stimulus phase cycle (-50 to 50%) for two stimulus duty cycles following an increase in force degradation cut-off to ≥70%, at (A) 8.6 s^{-1}, 69% cycle (sample size as in Fig. 5), and at (B) 8.6 s^{-1}, 50% cycle (n=1). Experimental parameters, symbols, colors, and the *in vivo* ranges of phases as in Fig. 6. Symbols for individual birds as in Fig. 2. (C-E) Summary statistics determined from the individual fits of the Generalized Additive Model, as in (E-G) in Fig. 6. Net power output by stimulus phase response curves of all treatments had a slope that differed significantly from zero (P< 0.05). Numbers indicate significant differences between the two stimulus duty cycle treatments, both tested at 8.6 s^{-1}. Percentage of initial force is included in brackets next to each subject's identification number.

Journal of Experimental Biology • Supplementary information

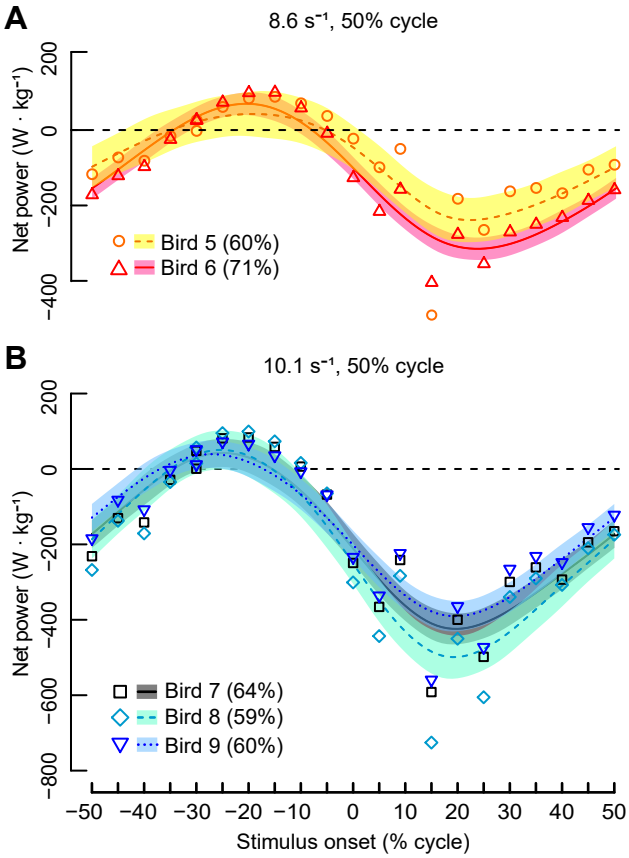

Fig. S3. The second sensitivity analysis demonstrates that trials with force degradation ≥59% have consistent work loop results. Net power output of the humerotriceps muscle across the full stimulus phase cycle (-50 to 50%) for (A) 8.6 s^{-1}, 50% stimulus cycle (Bird 5: yellow band and orange symbols/line; Bird 6: pink band and red symbols/line) and (B) 10.1 s^{-1}, 50% cycle (Bird 7: grey band and black symbols/lines; Bird 8: teal band and symbols/lines; Bird 9: light blue band and blue symbols/lines). Experimental parameters, and sample sizes, as in Fig. 5. Individual GAM fits are designated with different line types, and their respective 95% confidence intervals are indicated by coloured bands, both are coloured by individual. Percentage of initial force as in Fig. S2.

Journal of Experimental Biology • Supplementary information

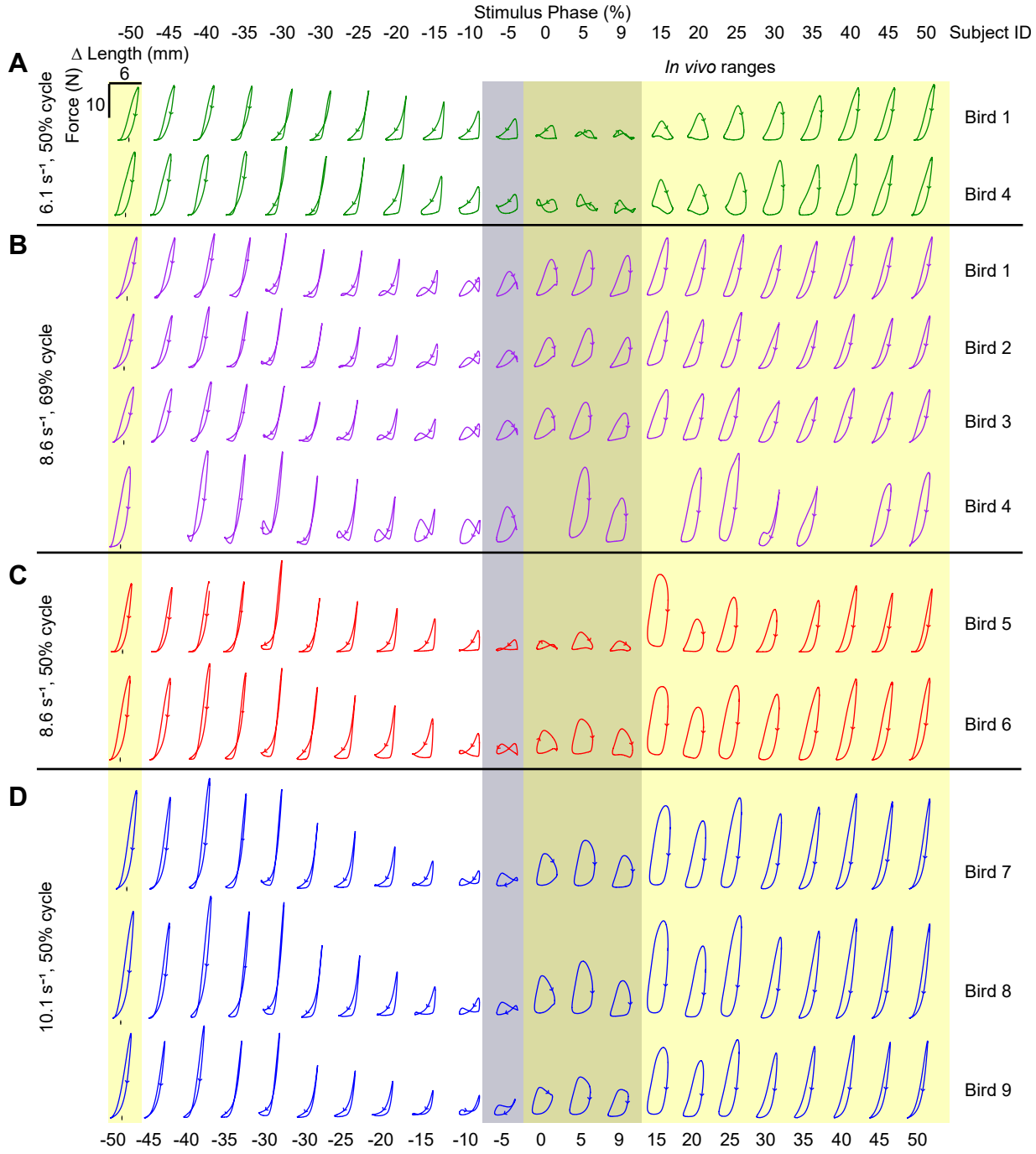

Fig. S4. Work loop results were consistent across individuals. The fourth work loop from all trials in the study are plotted as force (N) by length (Δ length mm) traces. The x-axis indicates stimulus onset phases (-50 to 50%) across all four experimental treatments. Arrows indicate the directionality of each work loop. Sample sizes, and colours for each treatment as in Fig. 5. (A) Work loop traces at 6.1 s^{-1} and 50% stimulus duty cycle. (B) Work loop traces at 8.6 s^{-1} and 69% stimulus duty cycle. (C) Work loop traces at 8.6 s^{-1} and 50% stimulus duty cycle. (D) Work loop traces at 10.1 s^{-1} and 50% stimulus duty cycle. Scale bars for both force and length are plotted with the upper-leftmost work loop (Bird 1, -50% phase) and apply to every work loop in the figure. The *in vivo* ranges of phases are highlighted in gray (Robertson and Biewener, 2012) and in yellow (Dial, 1992b).

Journal of Experimental Biology • Supplementary information